Observation of the Cosmic Microwave Background: The ESA Planck mission and Beyond

Martin BUCHER, Laboratoire Astroparticles & Cosmologie,
Université Paris 7 (Denis-Diderot)/CNRS
(for the Planck Collaboration)

12 October 2015, COSPA 2015 Daejeon, South Korea

The *Planck* mission

Planck timeline

- Proposal started in 1992
- Accepted by ESA in 1996
- Launch May 2009
- First release of results for cosmology (T only) March 2013
- Second release of results for cosmology
  (T and P except at low l) $\approx$ February 2015
- Finals cosmology results (mainly low-l P) (mid-2016)

A Joint Analysis of BICEP2/Keck Array and Planck Data BICEP2/Keck and Planck Collaborations 2015 Submitt
Planck intermediate results. XXX. The angular power spectrum of polarized dust emission at intermediate an
Planck 2015 results. I. Overview of products and results
Planck 2015 results. II. Low Frequency Instrument data processing
Planck 2015 results. III. LFI systematic uncertainties
Planck 2015 results. IV. LFI beams and window functions
Planck 2015 results. V. LFI calibration
Planck 2015 results. VI. LFI maps
Planck 2015 results. VII. High Frequency Instrument data processing: Time-ordered information and beam pro
Planck 2015 results. VIII. High Frequency Instrument data processing: Calibration and maps
Planck 2015 results. IX. Diffuse component separation: CMB maps
Planck 2015 results. X. Diffuse component separation: Foreground maps
Planck 2015 results. XI. CMB power spectra, likelihood, and consistency of cosmological parameters
Planck 2015 results. XII. Simulations Planck Collaboration
Planck 2015 results. XIII. Cosmological parameters
Planck 2015 results. XIV. Dark energy and modified gravity
Planck 2015 results. XV. Gravitational lensing
Planck 2015 results. XVI. Isotropy and statistics of the CMB
Planck 2015 results. XVII. Primordial non-Gaussianity
Planck 2015 results. XVIII. Background geometry and topology of the Universe
Planck 2015 results. XIX. Constraints on primordial magnetic fields
Planck 2015 results. XX. Constraints on inflation
Planck 2015 results. XXI. The integrated Sachs-Wolfe effect
Planck 2015 results. XXII. A map of the thermal Sunyaev-Zeldovich effect
Planck 2015 results. XXIII. Thermal Sunyaev-Zeldovich effect-cosmic infrared background correlation
Planck 2015 results. XXIV. Cosmology from Sunyaev-Zeldovich cluster counts
Planck 2015 results. XXV. Diffuse, low-frequency Galactic foregrounds
Planck 2015 results. XXVI. The Second Planck Catalogue of Compact Sources
Planck 2015 results. XXVII. The Second Planck Catalogue of Sunyaev-Zeldovich Sources
Planck 2015 results. XXVIII. The Planck Catalogue of Galactic Cold Clumps
http://www.cosmos.esa.int/web/planck/publications

PLANCK Focal Plane

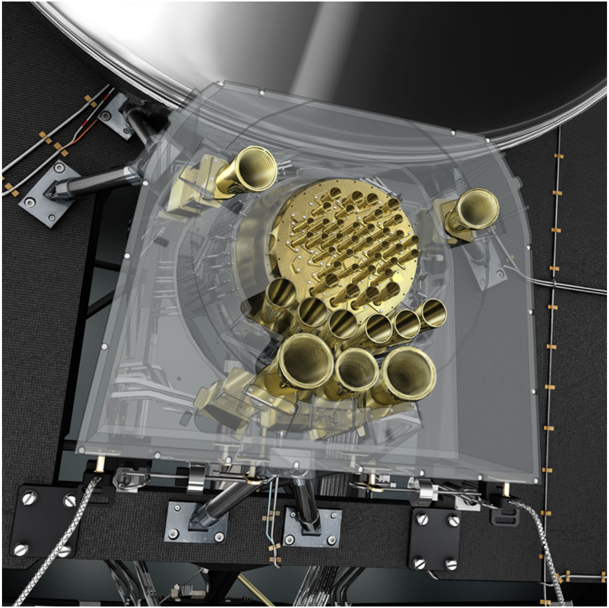

The workhorse of Planck : spiderweb and polarization sensitive bolometers

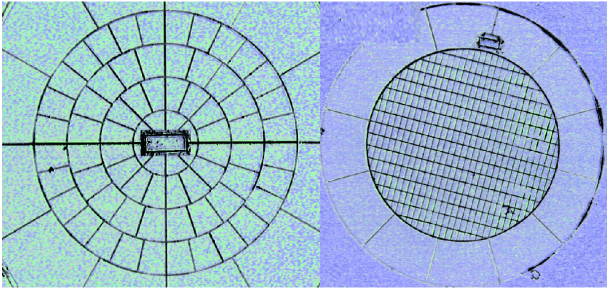

Made by JPL, Caltech
Cooled to $\approx 100mK$

Planck Capabilities

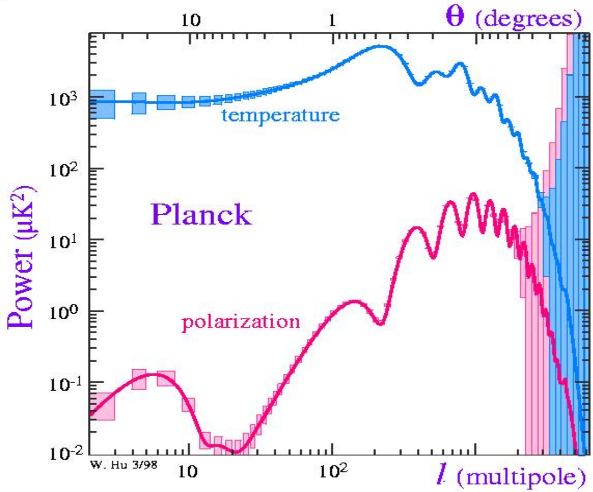

Planck Capabilities

Table 2. *Planck* performance parameters determined from flight data.

Channel	$N_{\text{detectors}}$ [a]	ν_{center} [b] [GHz]	Scanning Beam[c] FWHM [arcm]	Ellipticity	Noise[d] Sensitivity [$\mu K_{RJ}\, s^{1/2}$]	[$\mu K_{CMB}\, s^{1/2}$]
30 GHz	4	28.4	33.16	1.37	145.4	148.5
44 GHz	6	44.1	28.09	1.25	164.8	173.2
70 GHz	12	70.4	13.08	1.27	133.9	151.9
100 GHz	8	100	9.59	1.21	31.52	41.3
143 GHz	11	143	7.18	1.04	10.38	17.4
217 GHz	12	217	4.87	1.22	7.45	23.8
353 GHz	12	353	4.7	1.2	5.52	78.8
545 GHz	3	545	4.73	1.18	2.66	0.0259[d]
857 GHz	4	857	4.51	1.38	1.33	0.0259[d]

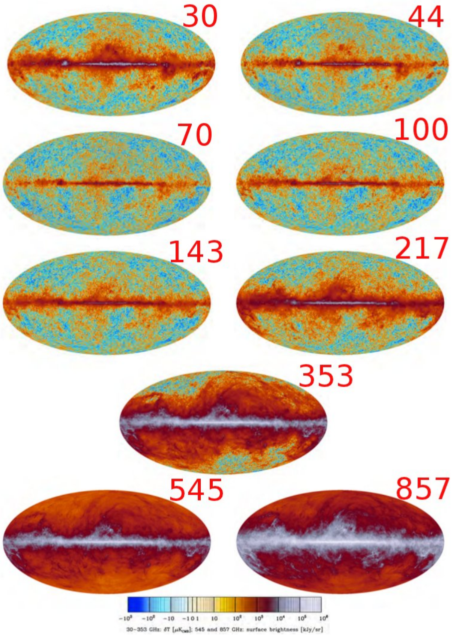
30
44
70
100
143
217
353
545
857
-10^3 -10^2 -10 -1 0 1 10 10^2 10^3 10^4 10^5 10^6
30–353 GHz: δT [μK_{CMB}]; 545 and 857 GHz: surface brightness [kJy/sr]

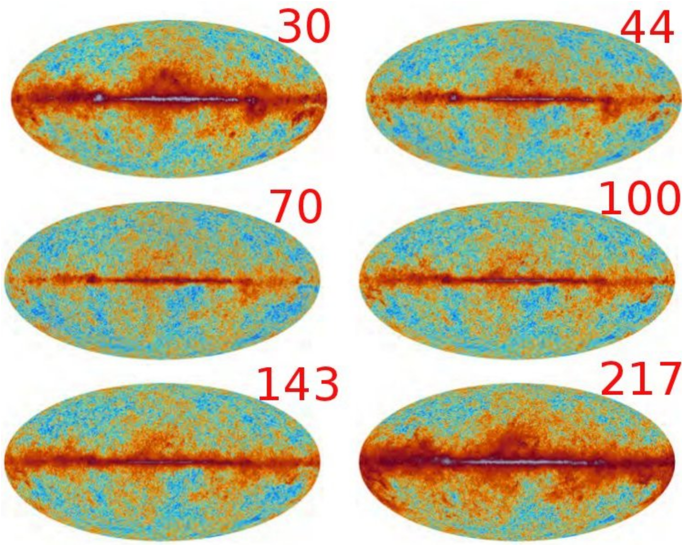
30
44
70
100
143
217

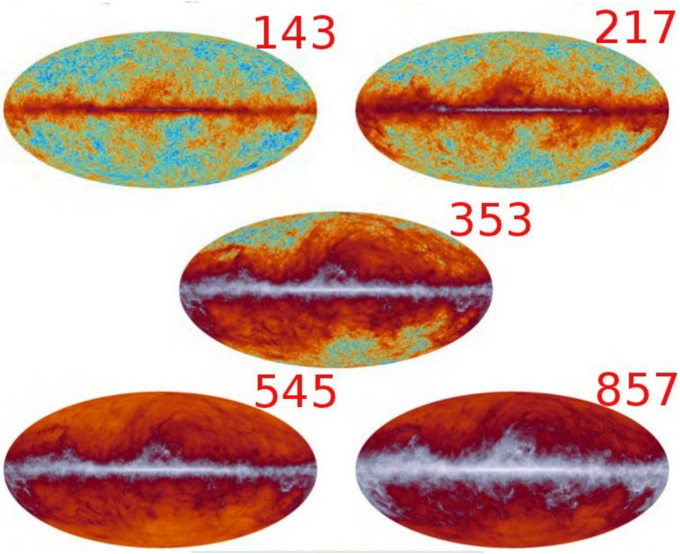
143
217
353
545
857

Planck ILC map

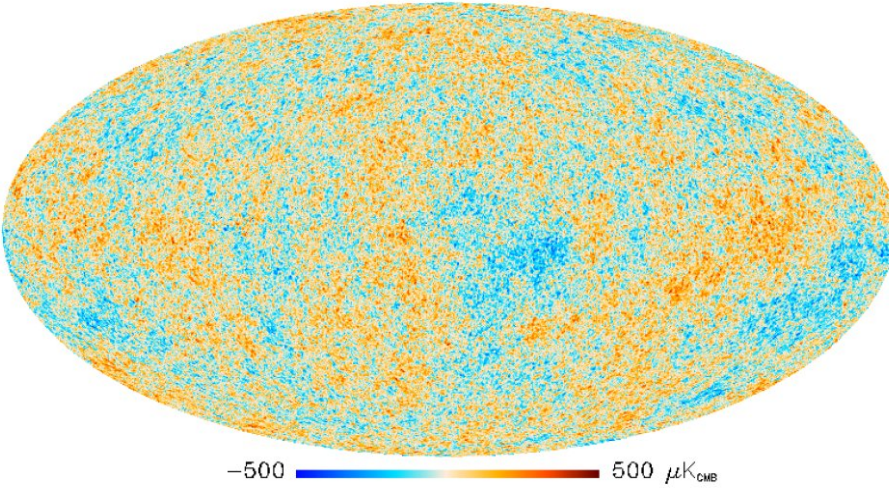

Theory – origin of the CMB anisotropy

Sachs-Wolfe formula

$$\frac{\delta T}{T}(\hat{\mathbf{n}}) = \left[\frac{1}{4}\delta_\gamma + \mathbf{v}_\gamma \cdot \mathbf{n} + \Phi i\right]_i^f + 2\int_i^f d\eta \frac{\partial \Phi'}{\partial \eta}(\eta, \hat{\mathbf{n}}(\eta_0 - \eta))$$

$\Phi \equiv \mathrm{Newtonian\ gravitational\ potential\ (dimensionless)}$

δ_γ and $\mathbf{v}_\gamma$ describe the fractional density contrast and peculiar 3-velocity of of the photon component.

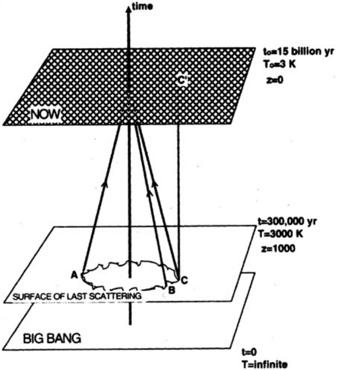

This treatment is somewhat naive because it assumes that the surface of last scatter is infinitely thin.
In reality the surface of last scatter has a width the smears the anisotropies on small scales.

The deadly sins of a non-inflationary universe.

1. Monopole problem
2. Horizon problem
3. Flatness problem
4. Smoothness problem

Single-Field Inflation

In the beginning there was a scalar field that dominated the universe. Everything came from this scalar field and there was nothing without the scalar field. The quantum fluctuations of this field (that is, those of the vacuum) generated small fluctuations that advanced or retarded the instant of re-heating. These were the seeds of the large-scale structure.

$$\ddot{\phi} + 3H\dot{\phi} = -V_{,\phi}$$

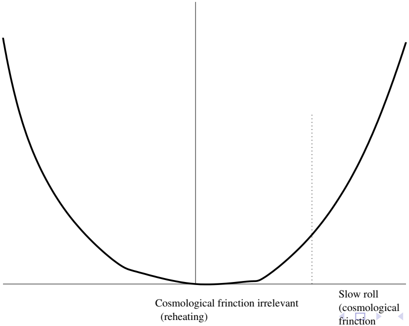

Massless scalar field in de Sitter space

$H_{phys} = \text{(constant)}.$

$$ds^2 = -\frac{1}{\eta^2}(-d\eta^2 + d\mathbf{x}^2), \qquad -\infty < \eta < 0.$$

$$S = \int \sqrt{-g}g^{\mu\nu}(\partial_\mu\phi)(\partial_\nu\phi) = \int d^4x\ a^2(\eta)\left[\left(\frac{\partial\phi}{\partial\eta}\right)^2 - (\nabla\phi)^2\right]$$

$$\frac{\partial^2\phi}{\partial\eta^2} - \frac{2}{\eta}\frac{\partial\phi}{\partial\eta} + k^2\phi = 0$$

Bessel equation

$$\phi(\eta) = \eta^{3/2}H^{(1)}_{3/2}(-k\eta)$$

$(k\eta) \approx 1$ horizon crossing.

Important points :

- Both the inflaton/scalar gravity degrees of freedom and the tensor metric perturbations exhbit the same qualitative behavior as the above idealized example.
- Modes fluctuation on subhorizon scales but become frozen in on superhorizon scales and stay frozen in until after the end of inflation.

Perturbations generated during inflation

$$\boxed{\hbar = c = 1, M_{pl}^{-2}} \qquad \delta\phi \approx H \qquad \frac{\delta\rho}{\bar\rho} \approx H \cdot \delta t, \quad \delta t \approx \frac{\delta\phi}{\dot\phi}$$

$$H\dot\phi \approx V_{,\phi}, \quad \dot\phi \approx V_{,\phi}/H, \quad H^2 \approx \frac{1}{M_{pl}^2} V, \frac{\delta\rho}{\bar\rho} \approx \frac{V^{3/2}[\phi(k)]}{M_{pl}^3 \ V_{,\phi}}$$

Scalar perturbations : $$\boxed{\mathcal{P}_S^{1/2}(k) \approx O(1) \cdot \frac{V^{3/2}[\phi(k)]}{M_{pl}^3 \ V_{,\phi}[\phi(k)]}.}$$

Tensor perturbations : $$\boxed{\mathcal{P}_T^{1/2}(k) \approx O(1) \cdot \frac{H}{M_{pl}} \approx O(1) \cdot \frac{V^{1/2}}{M_{pl}^2}}$$

$\phi(k) \equiv$ value of ϕ at horizon crossing of the mode k

Reconstruction of the inflationary potential : the tensors measure the height of the potential, the scalars the slope.

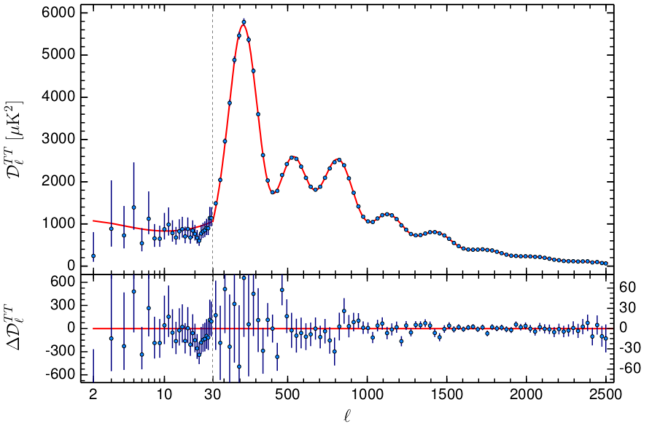

Fig. 1. The *Planck* 2015 temperature power spectrum. At multipoles $\ell \geq 30$ we show the maximum likelihood frequency averaged temperature spectrum computed from the `Plik` cross-half-mission likelihood with foreground and other nuisance parameters determined from the MCMC analysis of the base ΛCDM cosmology. In the multipole range $2 \leq \ell \leq 29$, we plot the power spectrum estimates from the `Commander` component-separation algorithm computed over 94% of the sky. The best-fit base ΛCDM theoretical spectrum fitted to the *Planck* TT+lowP likelihood is plotted in the upper panel. Residuals with respect to this model are shown in the lower panel. The error bars show $\pm 1\,\sigma$ uncertainties.

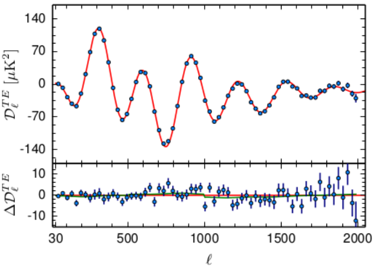

$\mathcal{D}_\ell^{TE}$ [μK^2]
140
70
0
-70
-140
$\Delta\mathcal{D}_\ell^{TE}$
10
0
-10
30
500
1000
1500
2000
ℓ

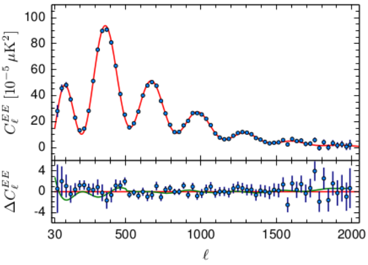

C_ℓ^{EE} [10^{-5} μK^2]
100
80
60
40
20
0
ΔC_ℓ^{EE}
4
0
-4
30
500
1000
1500
2000
ℓ

The six-parameter concordance model

[1] Parameter	[2] 2013N(DS)	[3] 2013F(DS)	[4] 2013F(CY)	[5] 2015F(CHM)	[6] 2015F(CHM) (Plik)	$([2]-[6])/\sigma_{[6]}$	$([5]-[6])/\sigma_{[5]}$
$100\theta_{MC}$	1.04131 ± 0.00063	1.04126 ± 0.00047	1.04121 ± 0.00048	1.04094 ± 0.00048	1.04086 ± 0.00048	0.71	0.17
$\Omega_b h^2$	0.02205 ± 0.00028	0.02234 ± 0.00023	0.02230 ± 0.00023	0.02225 ± 0.00023	0.02222 ± 0.00023	−0.61	0.13
$\Omega_c h^2$	0.1199 ± 0.0027	0.1189 ± 0.0022	0.1188 ± 0.0022	0.1194 ± 0.0022	0.1199 ± 0.0022	0.00	−0.23
H_0	67.3 ± 1.2	67.8 ± 1.0	67.8 ± 1.0	67.48 ± 0.98	67.26 ± 0.98	0.03	0.22
n_s	0.9603 ± 0.0073	0.9665 ± 0.0062	0.9655 ± 0.0062	0.9682 ± 0.0062	0.9652 ± 0.0062	−0.67	0.48
Ω_m	0.315 ± 0.017	0.308 ± 0.013	0.308 ± 0.013	0.313 ± 0.013	0.316 ± 0.014	−0.06	−0.23
σ_8	0.829 ± 0.012	0.831 ± 0.011	0.828 ± 0.012	0.829 ± 0.015	0.830 ± 0.015	−0.08	−0.07
τ	0.089 ± 0.013	0.096 ± 0.013	0.094 ± 0.013	0.079 ± 0.019	0.078 ± 0.019	0.85	0.05
$10^9 A_s e^{-2\tau}$	1.836 ± 0.013	1.833 ± 0.011	1.831 ± 0.011	1.875 ± 0.014	1.881 ± 0.014	−3.46	−0.42

Parameterization of primordial power spectrum used here :

$$P(k) = A_S (k/k_p)^{ns}$$

Table 5. Constraints on 1-parameter extensions to the base ΛCDM model for combinations of *Planck* power spectra, *Planck* lensing, and external data (BAO+JLA+H_0, denoted "ext"). Note that we quote 95 % limits here.

Parameter	TT	TT+lensing	TT+lensing+ext	TT, TE, EE	TT, TE, EE+lensing	TT, TE, EE+lensing+ext
Ω_K	$-0.052^{+0.049}_{-0.055}$	$-0.005^{+0.016}_{-0.017}$	$-0.0001^{+0.0054}_{-0.0052}$	$-0.040^{+0.038}_{-0.041}$	$-0.004^{+0.015}_{-0.015}$	$0.0008^{+0.0040}_{-0.0039}$
Σm_ν [eV]	< 0.715	< 0.675	< 0.234	< 0.492	< 0.589	< 0.194
$N_{\rm eff}$	$3.13^{+0.64}_{-0.63}$	$3.13^{+0.62}_{-0.61}$	$3.15^{+0.41}_{-0.40}$	$2.99^{+0.41}_{-0.39}$	$2.94^{+0.38}_{-0.38}$	$3.04^{+0.33}_{-0.33}$
$Y_{\rm P}$	$0.252^{+0.041}_{-0.042}$	$0.251^{+0.040}_{-0.039}$	$0.251^{+0.035}_{-0.036}$	$0.250^{+0.026}_{-0.027}$	$0.247^{+0.026}_{-0.027}$	$0.249^{+0.025}_{-0.026}$
$dn_s/d\ln k$	$-0.008^{+0.016}_{-0.016}$	$-0.003^{+0.015}_{-0.015}$	$-0.003^{+0.015}_{-0.014}$	$-0.006^{+0.014}_{-0.014}$	$-0.002^{+0.013}_{-0.013}$	$-0.002^{+0.013}_{-0.013}$
$r_{0.002}$	< 0.103	< 0.114	< 0.114	< 0.0987	< 0.112	< 0.113
w	$-1.54^{+0.62}_{-0.50}$	$-1.41^{+0.64}_{-0.56}$	$-1.006^{+0.085}_{-0.091}$	$-1.55^{+0.58}_{-0.48}$	$-1.42^{+0.62}_{-0.56}$	$-1.019^{+0.075}_{-0.080}$

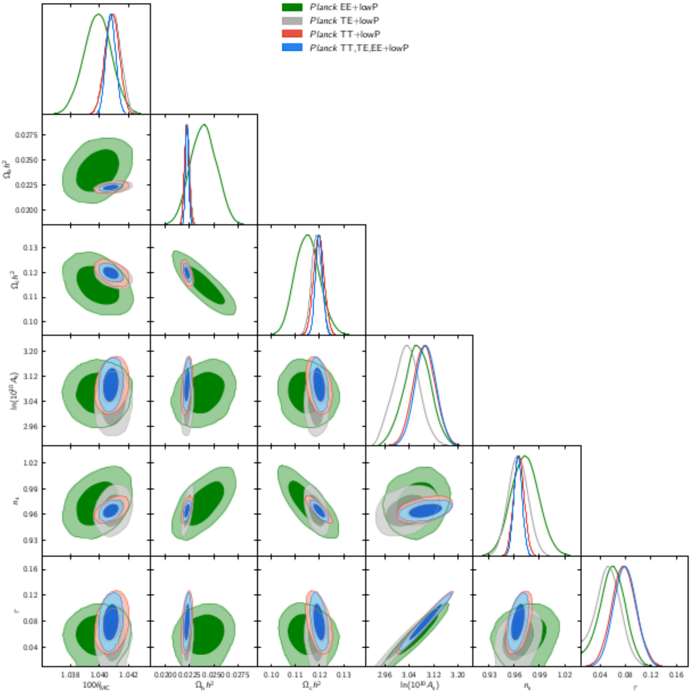

Planck EE+lowP
Planck TE+lowP
Planck TT+lowP
Planck TT,TE,EE+lowP
$100\theta_{MC}$
$\Omega_b h^2$
$\Omega_c h^2$
$\ln(10^{10} A_s)$
n_s
τ

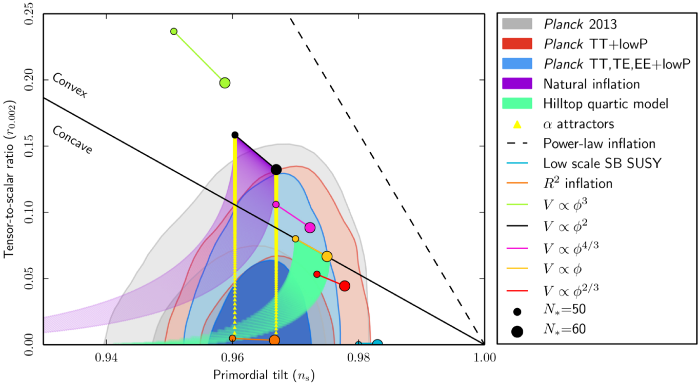

Fig. 12. Marginalized joint 68 % and 95 % CL regions for n_s and $r_{0.002}$ from *Planck* in combination with other data sets, compared to the theoretical predictions of selected inflationary models.

Table 6. Results of the inflationary model comparison. We provide $\Delta\chi^2$ with respect to base ΛCDM and Bayes factors with respect to R^2 inflation.

Inflationary model	$\Delta\chi^2$		$\ln B_{0X}$	
	$w_{\rm int} = 0$	$w_{\rm int} \neq 0$	$w_{\rm int} = 0$	$w_{\rm int} \neq 0$
$R + R^2/(6M^2)$	+0.8	+0.3	...	+0.7
$n = 2/3$	+6.5	+3.5	−2.4	−2.3
$n = 1$	+6.2	+5.5	−2.1	−1.9
$n = 4/3$	+6.4	+5.5	−2.6	−2.4
$n = 2$	+8.6	+8.1	−4.7	−4.6
$n = 3$	+22.8	+21.7	−11.6	−11.4
$n = 4$	+43.3	+41.7	−23.3	−22.7
Natural	+7.2	+6.5	−2.4	−2.3
Hilltop ($p = 2$)	+4.4	+3.9	−2.6	−2.4
Hilltop ($p = 4$)	+3.7	+3.3	−2.8	−2.6
Double well	+5.5	+5.3	−3.1	−2.3
Brane inflation ($p = 2$)	+3.0	+2.3	−0.7	−0.9
Brane inflation ($p = 4$)	+2.8	+2.3	−0.4	−0.6
Exponential inflation	+0.8	+0.3	−0.7	−0.9
SB SUSY	+0.7	+0.4	−2.2	−1.7
Supersymmetric α-model	+0.7	+0.1	−1.8	−2.0
Superconformal ($m = 1$)	+0.9	+0.8	−2.3	−2.2
Superconformal ($m \neq 1$)	+0.7	+0.5	−2.4	−2.6

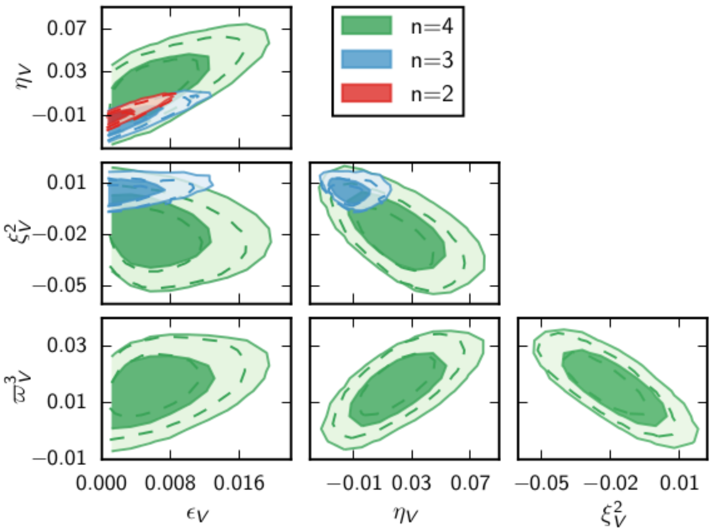

Fig. 13. Posterior distributions for the first four potential slow-roll parameters when the potential is Taylor-expanded to nth order, using *Planck* TT+lowP+BAO (filled contours) or TT,TE,EE+lowP (dashed contours). The primordial spectra are computed *beyond* any slow-roll approximation.

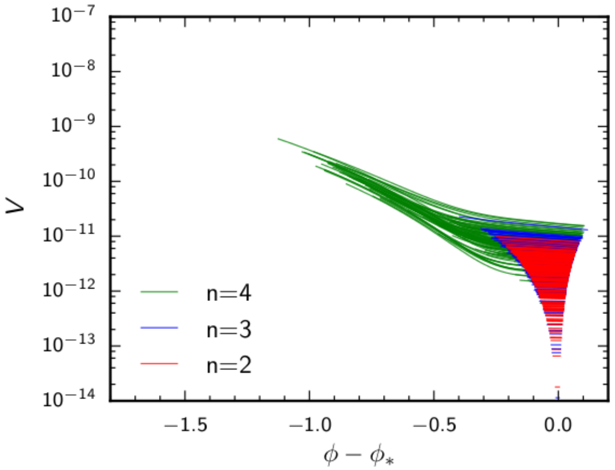

Fig. 15. Observable range of the best-fit inflaton potentials, when $V(\phi)$ is Taylor expanded to the nth order around the pivot value ϕ_*, in natural units (where $\sqrt{8\pi}M_{\rm pl} = 1$), assuming a flat prior on $\epsilon_V, \eta_V, \xi_V^2$, and ϖ_V^3, and using *Planck* TT+lowP+BAO. Potentials obtained under the transformation $(\phi - \phi_*) \rightarrow (\phi_* - \phi)$ leave the same observable signature and are also allowed. The sparsity of potentials with a small $V_0 = V(\phi_*)$ comes from the flat prior on ϵ_V rather than on $\ln(V_0)$; in fact, V_0 is unbounded from below in

Underlying question : conventional parameterization

What is the primordial power spectrum ?

- For lack of a fundamental theory, expand in powers of $\ln(k)$

$$
\begin{aligned}
\ln\left(\mathcal{P}(\ln k)\right) &= \mathcal{P}_0\left(\ \ln(k/k_{piv})\right)^0 + \mathcal{P}_1\left(\ \ln(k/k_{piv})\right)^1 + \mathcal{P}_2\left(\ \ln(k/k_{piv})\right)^2 + \dots \\
\mathcal{P}(k) &= A(k/k_{piv})^{(n_s-1)} \\
&\text{or} \\
\mathcal{P}(k) &= A(k/k_{piv})^{(n_s-1)+\alpha\ln(k/k_{piv})+\dots}
\end{aligned}
$$

- *Planck* seems to be telling us that the first two terms suffice, and using just the first term can be ruled out at a respectable statistical significance. $n_S \neq 1$ implies exact scale invariance needs to be downgraded to an approximate symmetry. No statistically significant evidence for running of the spectral index.

$$
\begin{aligned}
\mathbf{f}^{\mathrm{T}}\mathbf{R}(\lambda,\alpha)\mathbf{f} \equiv \lambda \int \mathrm{d}\kappa \left(\frac{\partial^2 f(\kappa)}{\partial\kappa^2}\right)^2 \\
+ \alpha \int_{-\infty}^{\kappa_{\min}} \mathrm{d}\kappa\, f^2(\kappa) + \alpha \int_{\kappa_{\max}}^{+\infty} \mathrm{d}\kappa\, f^2(\kappa).
\end{aligned}
$$

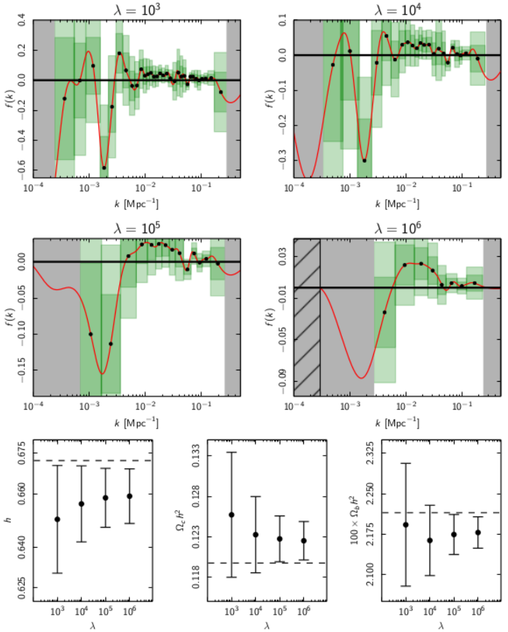

Fig. 21. *Planck* TT likelihood primordial power spectrum (PPS)

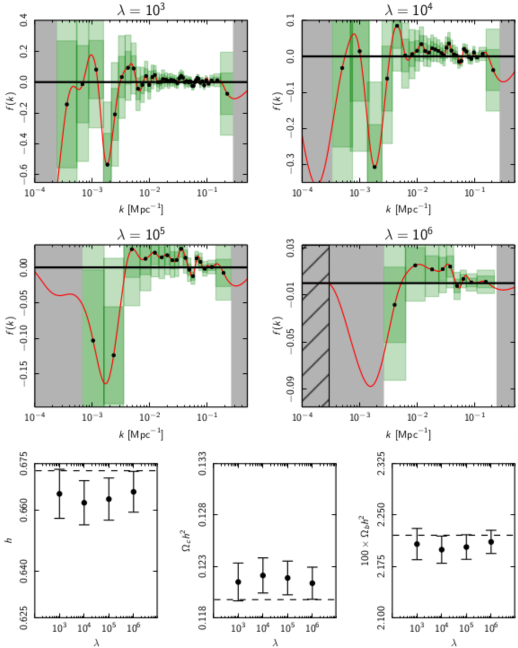

Fig. 22. *Planck* TT,TE,EE+lowTEB likelihood primordial power spectrum reconstruction results. *Top four panels:*

Planck Gravitational lensing spectrum

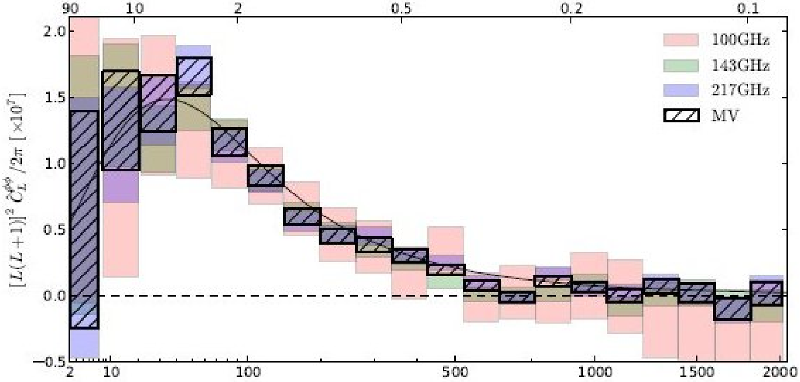

Fig. 18. Fiducial lensing power spectrum estimates based on the 100, 143, and 217 GHz frequency reconstructions, as well as the minimum-variance reconstruction that forms the basis for the *Planck* lensing likelihood.

Planck 2013 Results. XXIV. Constraints on primordial non-Gaussianity

Planck Collaboration : P. A. R. Ade, N. Aghanim, C. Armitage-Caplan, M. Arnaud, M. Ashdown, F. Atrio-Barandela, J. Aumont, C. Baccigalupi, A. J. Banday, R. B. Barreiro, J. G. Bartlett, N. Bartolo, E. Battaner, K. Benabed, A. Benoît, A. Benoit-Lévy, J.-P. Bernard, M. Bersanelli, P. Bielewicz, J. Bobin, J. J. Bock, A. Bonaldi, L. Bonavera, J. R. Bond, J. Borrill, F. R. Bouchet, M. Bridges, M. Bucher, C. Burigana, R. C. Butler, J.-F. Cardoso, A. Catalano, A. Challinor, A. Chamballu, L.-Y Chiang, H. C. Chiang, P. R. Christensen, S. Church, D. L. Clements, S. Colombi, L. P. L. Colombo, F. Couchot, A. Coulais, B. P. Crill, A. Curto, F. Cuttaia, R. D. Davies, R. J. Davis, P. de Bernardis, A. de Rosa, G. de Zotti, J. Delabrouille, J.-M. Delouis, F.-X. Désert, J. M. Diego, H. Dole, S. Donzelli, et al. (175 additional authors not shown) (Submitted on 20 Mar 2013)

The Planck nominal mission cosmic microwave background (CMB) maps yield unprecedented constraints on primordial non-Gaussianity (NG). Using three optimal bispectrum estimators, separable template-fitting (KSW), binned, and modal, we obtain consistent values for the primordial local, equilateral, and orthogonal bispectrum amplitudes, quoting as our final result $f_{NL}^{local} = 2.7 \pm 5.8$, $f_{NL}^{equil} = -42 \pm 75$, and $f_{NL}^{ortho} = -25 \pm 39$ (68% CL statistical) ; and we find the integrated Sachs-Wolfe lensing bispectrum expected in the ΛCDM scenario. The results are based on comprehensive cross-validation of these estimators on Gaussian and non-Gaussian simulations, are stable across component separation techniques, pass an extensive suite of tests, and are confirmed by skew-C_l, wavelet bispectrum and Minkowski functional estimators. Beyond estimates of individual shape amplitudes, we present model-independent, three-dimensional reconstructions of the Planck CMB bispectrum and thus derive constraints on early-Universe scenarios that generate primordial NG, including general single-field models of inflation, excited initial states (non-Bunch-Davies vacua), and directionally-dependent vector models. We provide an initial survey of scale-dependent feature and resonance models. These results bound both general single-field and multi-field model parameter ranges, such as the speed of sound, $c_s \geq 0.02 (95\% CL)$, in an effective field theory parametrization, and the curvaton decay fraction $r_D \geq 0.15 (95\% CL)$. The Planck data put severe pressure on ekpyrotic/cyclic scenarios. The amplitude of the four-point function in the local model $\tau_{NL} < 2800 (95\% CL)$. Taken together, these constraints represent the highest precision tests to date of physical mechanisms for the origin of cosmic structure.

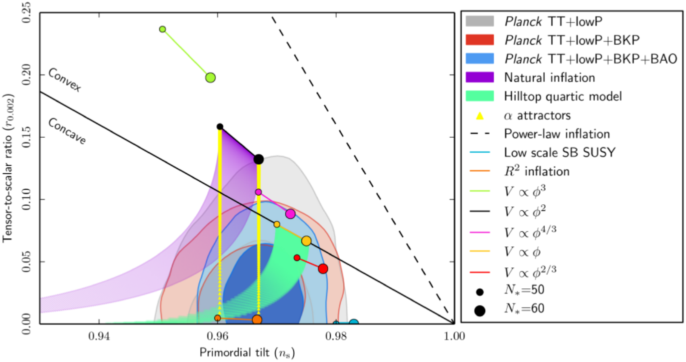

Fig. 54. Marginalized joint 68 % and 95 % CL regions for n_s and $r_{0.002}$ from *Planck* alone and in combination with its cross-correlation with BICEP2/Keck Array and/or BAO data compared with the theoretical predictions of selected inflationary models.

SEARCHING FOR B MODES

E and B Mode Polarization

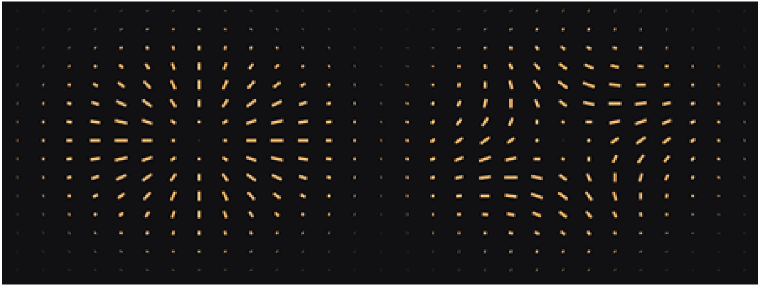

E mode B mode

$$\mathbf{Y}^{(E)}_{\ell m,ab} = \sqrt{\frac{2}{(\ell-1)\ell(\ell+1)(\ell+2)}}\left[\nabla_a\nabla_b - \frac{1}{2}\delta_{ab}\nabla^2\right]Y_{\ell m}(\hat{\Omega})$$

$$\mathbf{Y}^{(B)}_{\ell m,ab} = \sqrt{\frac{2}{(\ell-1)\ell(\ell+1)(\ell+2)}}\frac{1}{2}\left[\epsilon_{ac}\nabla_c\nabla_b + \nabla_a\epsilon_{bc}\nabla_c\right]Y_{\ell m}(\hat{\Omega})$$

Projection of « scalars, »« vectors »and « tensors »onto the celestial sphere

Under projection onto the celestial sphere :

$$(scalar)_3 \to (scalar)_2,$$

$$(vector)_3 \to (scalar)_2 + (vector)_2,$$

$$(tensor)_3 \to (scalar)_2 + (vector)_2.$$

There is no $(tensor)_2$ component. The E mode polarization is scalar ; the B mode is vector.

It follows that at linear order the scalar modes cannot generate any B mode polarization.

$\boxed{\text{Note crucial role of linearity assumption.}}$

Inflationary Prediction for Scalar & Tensor Anisotropies

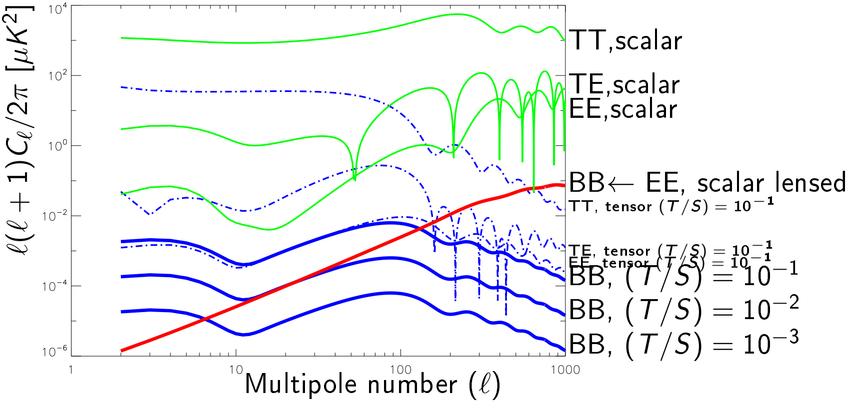

The Reionization Bump

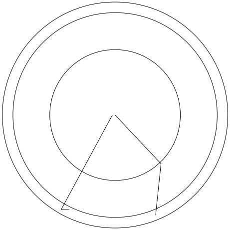

It turns out that

$$P \propto (1-\tau) d_{lastscatter}^2 \frac{\partial^2 T}{\partial x^2}$$

is small compared to

$$P \propto \tau d_{reion}^2 \frac{\partial^2 T}{\partial x^2}$$

even when τ is small.

Breaking news 22 March 2014

The Economist

World politics | Business & finance | Economics | Science & technology | Culture

Astrophysics

BICEP flexes its muscles

A telescope at the South Pole has made the biggest cosmological discovery so far this century

Mar 22nd 2014 | From the print edition

Timekeeper | Like 204 | Tweet 39

Keith Vanderlinde/National Science Foundation

ONE useful feature of a scientific theory is that it makes testable predictions. Such predictions, though, do not have to be testable straight away. Physics is replete with prophecies that could be confirmed or denied only decades later, once the technology to examine them had caught up. The Higgs boson, for example, was 50 years in the confirming.

BICEP2 summary plot :

"Smoking gun" of gravitational waves from inflation ?

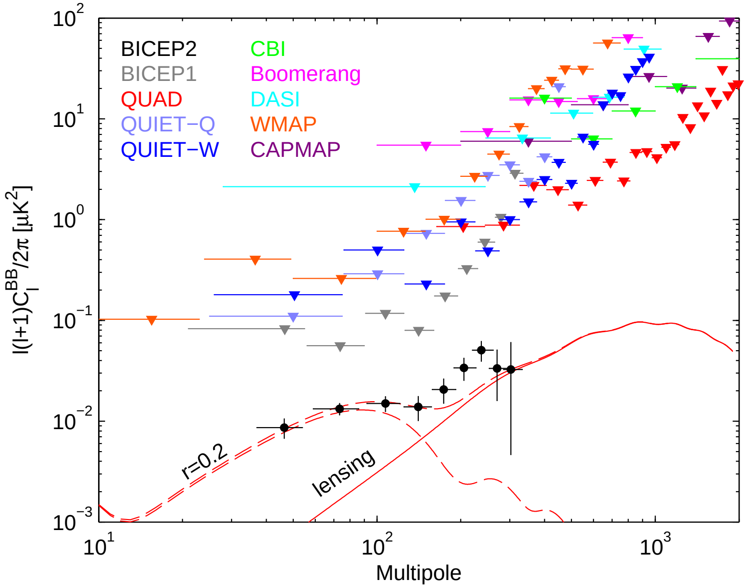

Why they said that dust cannot explain observed signal ?

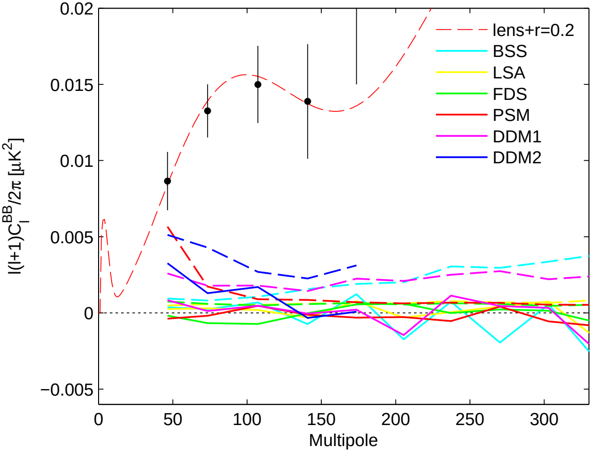

Was this celebration premature ?

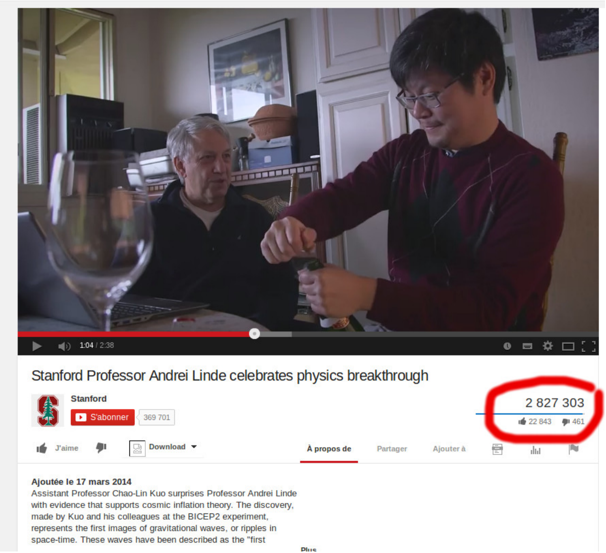

Detecting tensor modes with the CMB

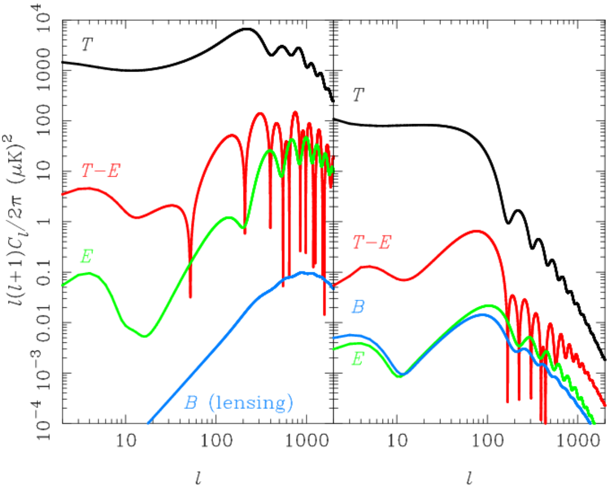

r=0.24

Taken from : Challinor, astro-ph/1210.6008

BICEP2 claim on Planck-like plot

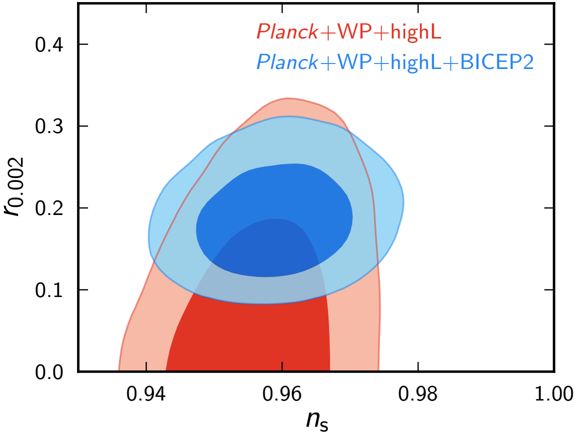

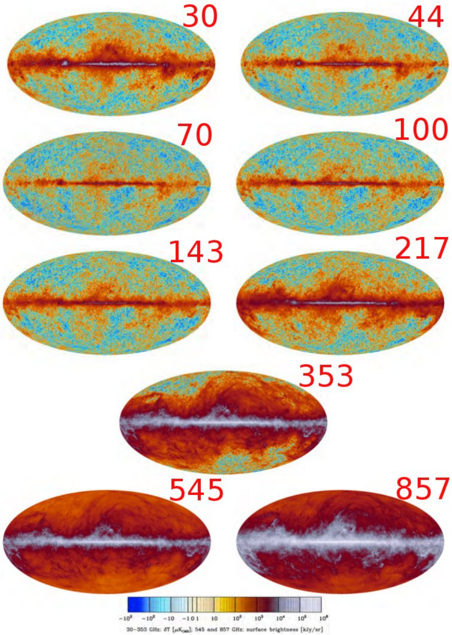
30
44
70
100
143
217
353
545
857
-10^3 -10^2 -10 -1 0 1 10 10^2 10^3 10^4 10^5 10^6
30–353 GHz: δT [μK_{CMB}]; 545 and 857 GHz: surface brightness [kJy/sr]

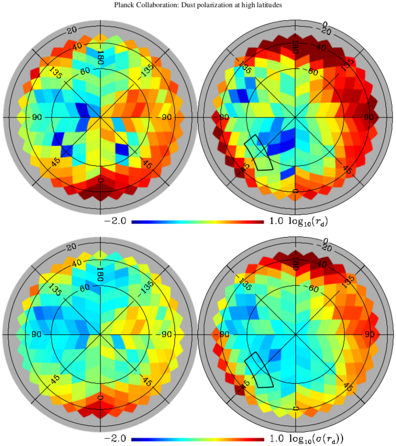

From Planck Collaboration : Dust polarization at high latitudes (astro-ph/1409.3738)

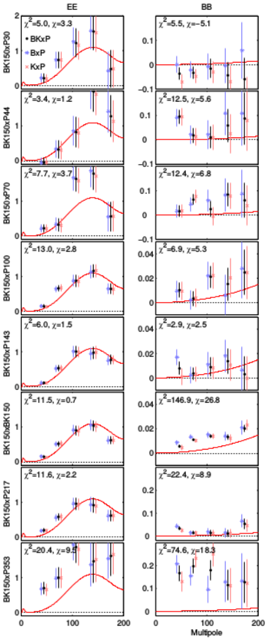

EE
BB
BK150xP30
BK150xP44
BK150xP70
BK150xP100
BK150xP143
BK150xBK150
BK150xP217
BK150xP353
χ²=5.0, χ=3.3
BKxP
BxP
KxP
χ²=5.5, χ=−5.1
χ²=3.4, χ=1.2
χ²=12.5, χ=5.6
χ²=7.7, χ=3.7
χ²=12.4, χ=6.8
χ²=13.0, χ=2.8
χ²=6.9, χ=5.3
χ²=6.0, χ=1.5
χ²=2.9, χ=2.5
χ²=11.5, χ=0.7
χ²=146.9, χ=26.8
χ²=11.6, χ=2.2
χ²=22.4, χ=8.9
χ²=20.4, χ=9.5
χ²=74.6, χ=18.3
Multipole

r<0.12 at 95 % now from B modes

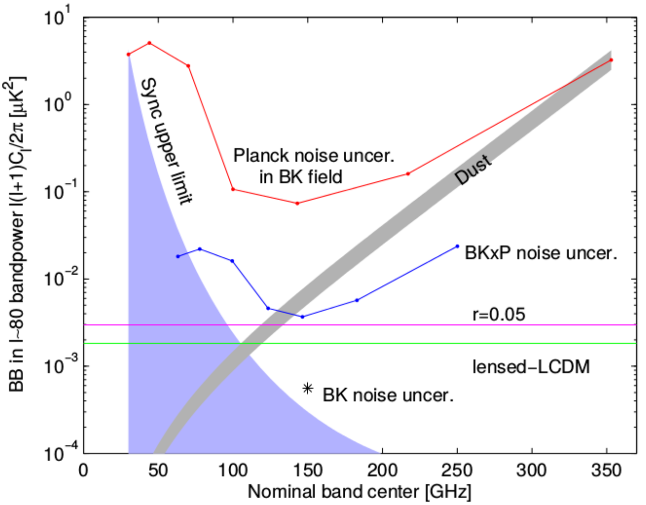

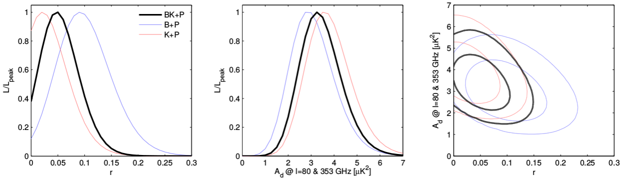

FIG. 6. Likelihood results from a basic lensed-ΛCDM+r+dust model, fitting BB auto- and cross-spectra taken between maps at 150 GHz, 217, and 353 GHz. The 217 and 353 GHz maps come from *Planck*. The primary results (heavy black) use the 150 GHz combined maps from BICEP2/*Keck*. Alternate curves (light blue and red) show how the results vary when the BICEP2 and *Keck Array* only maps are used. In all cases a Gaussian prior is placed on the dust frequency spectrum parameter $\beta_{\rm d} = 1.59 \pm 0.11$. In the right panel the two dimensional contours enclose 68% and 95% of the total likelihood.

COrE : Cosmic Origins Explorer

A space mission for measuring microwave band polarization on the full sky

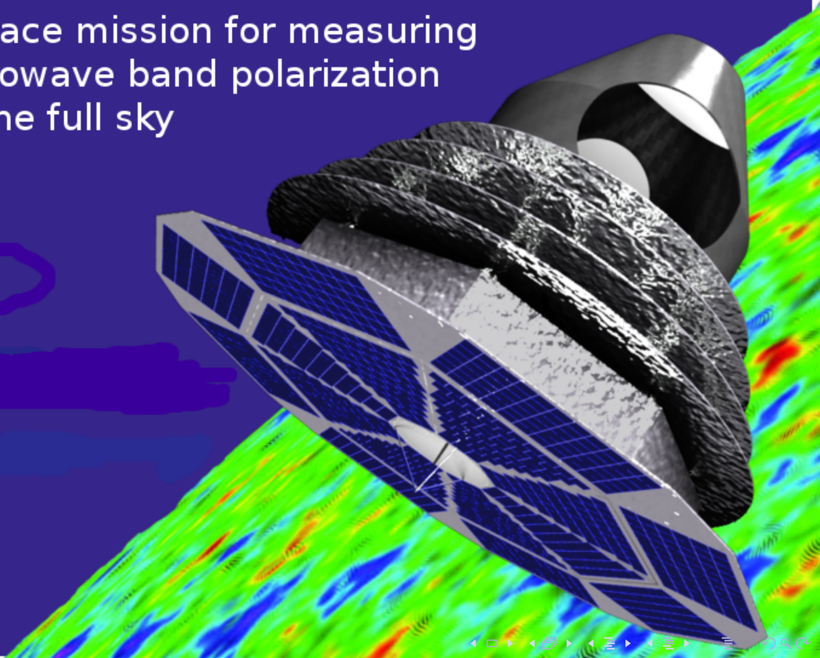

COrE Focal Plane (6384 detectors)

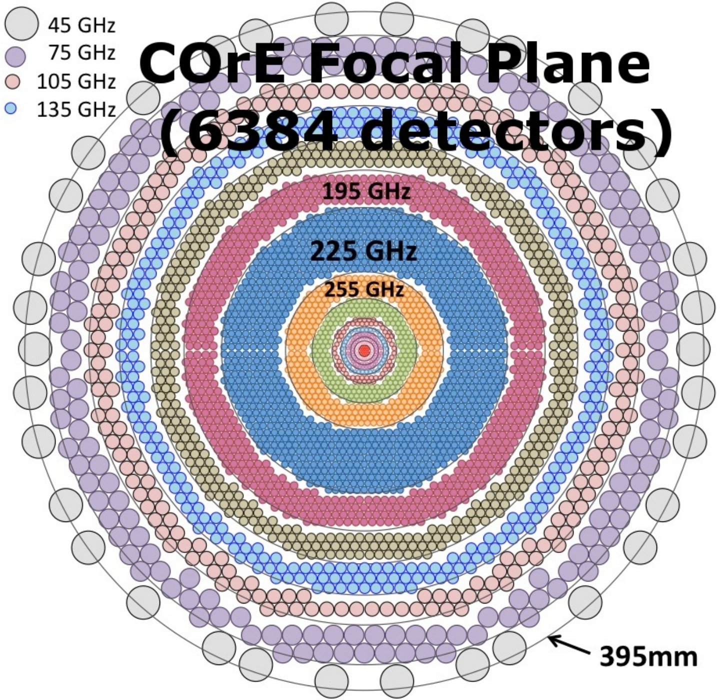

ビッグバン以前の宇宙を探るLiteBIRD衛星

Lite (light) Satellite for the studies of **B**-mode polarization and **I**nflation from cosmic background **R**adiation **D**etection

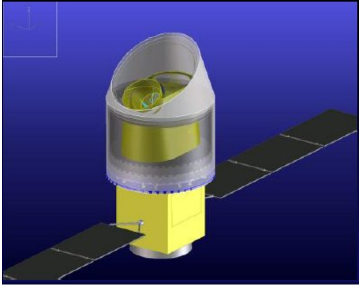

高エネルギー加速器研究機構(KEK)
素粒子原子核研究所
宇宙背景放射(CMB)実験グループ
羽澄昌史(はずみまさし)
for the LiteBIRD Working Group

第1回小型科学衛星シンポジウム
2011年3月1日

This talk is dedicated to Bruce Winstein.

LiteBird Detectors/Resolution

Band	Beam size [degs]	Pixel size[cm]	Edge Taper [dB]	Aperture efficiency	The # of bolometers	uK arcmin for 2 K mirror/baffle
60	1.7	2.0	4.5	0.65	312	6.35
80	1.3	2.0	7.8	0.84	156	6.53
100	1	2.0	<-10	0.94	156	6.06
Sub total					624	
100	1	1.2	-4.5	0.65	434	4.16
150	0.7	1.2	-10	0.91	434	3.02
220	0.47	1.2	<-10	0.99	434	3.02
Sub total					1302	
Total					**1926**	**1.7**

For more details on the CMB :

arXiv:1501.04288v1 [astro-ph.CO] 18 Jan 2015

Physics of the cosmic microwave background anisotropy*

Martin Bucher
Laboratoire APC, Université Paris 7/CNRS
Bâtiment Condorcet, Case 7020
75205 Paris Cedex 13, France
bucher@apc.univ-paris7.fr and
Astrophysics and Cosmology Research Unit
School of Mathematics, Statistics and Computer Science
University of KwaZulu-Natal
Durban 4041, South Africa

January 20, 2015

Abstract

Observations of the cosmic microwave background (CMB), especially of its frequency spectrum and its anisotropies, both in temperature and in polarization, have played a key role in the development of modern cosmology and our understanding of the very early universe. We review the underlying physics of the CMB and how the primordial temperature and polarization anisotropies were imprinted. Possibilities for distinguishing competing cosmological models are emphasized. The current status of CMB experiments and experimental techniques with an emphasis toward future observations, particularly in polarization, is reviewed. The physics of foreground emissions, especially of polarized dust, is discussed in detail, since this area is likely to become crucial for measurements of the B modes of the CMB polarization at ever greater sensitivity.